The Astronomical Journal, 146:158 (10pp), 2013 December doi:10.1088/0004-6256/146/6/158

H I LYMAN-ALPHA EQUIVALENT WIDTHS OF STELLAR POPULATIONS

María A. Peña-Guerrero and Claus Leitherer
Space Telescope Science Institute, 3700 San Martin Drive, Baltimore, MD 21218, USA; pena@stsci.edu, leitherer@stsci.edu
Received 2013 July 11; accepted 2013 October 1; published 2013 November 11

ABSTRACT

We have compiled a library of stellar Lyman-alpha (Lyα) equivalent widths in O and B stars using the model atmosphere codes CMFGEN and TLUSTY, respectively. The equivalent widths range from about 0 to 30 Å in absorption for early-O to mid-B stars. The purpose of this library is for the prediction of the underlying stellar Lyα absorption in stellar populations of star-forming galaxies with nebular Lyα emission. We implemented the grid of individual equivalent widths into the Starburst99 population synthesis code to generate synthetic Lyα equivalent widths for representative star formation histories. A starburst observed after 10 Myr will produce a stellar Lyα line with an equivalent width of $\sim -10 \pm 4$ Å in absorption for a Salpeter initial mass function. The lower value (deeper absorption) results from an instantaneous burst, and the higher value (shallower line) from continuous star formation. Depending on the escape fraction of nebular Lyα photons, the effect of stellar Lyα on the total profile ranges from negligible to dominant. If the nebular escape fraction is 10%, the stellar absorption and nebular emission equivalent widths become comparable for continuous star formation at ages of 10–20 Myr.

Key words: galaxies: star formation – stars: early-type

Online-only material: color figures

1. INTRODUCTION

Galaxies with active star formation host large populations of massive, hot, young O and B stars which ionize the surrounding interstellar medium (ISM). The resulting nebular recombination spectrum includes numerous strong emission lines which are widely used as star formation tracers (Kennicutt & Evans 2012). Among these lines, Lyman-alpha (Lyα) deserves special attention. Lyα photons are expected to be produced when the opacity approaches infinity for those photons associated with the base level (Case B). Hence, if Case B applies, strong Lyα emission is expected, and this line can be detected even at the highest redshifts (i.e., Partridge & Peebles 1967; Malhotra & Rhoads 2002; Stern et al. 2005; Bromm & Yoshida 2011; Sandberg et al. 2013, and references therein).

At high redshift, Lyα is often the only detectable emission line in the optical and near-infrared, and is therefore widely used as an indicator of star formation (i.e., Malhotra & Rhoads 2002; Scarlata et al. 2009; Dijkstra & Wyithe 2012). If the continuum light is detected, the Lyα equivalent width (EW) can give valuable clues on population ages and the stellar initial mass function (IMF; Leitherer et al. 2010). If Case B applies, the theoretically predicted values of EWs are expected to vary from 50 to ~240 Å in star-forming galaxies with ages of less than 100 Myr (i.e., Charlot & Fall 1993; Laursen et al. 2013, and references therein). However, Lyα turns out to be a complex star formation tracer. In most cases, the observed line strength is less than expected from Case B recombination because the effects of radiation transfer have not been taken into account (Hansen & Oh 2006). The assumption of Lyα being a pure recombination line in a gaseous medium is too simple. Meier & Terlevich (1981), Hartmann et al. (1988), Neufeld (1990), and Charlot & Fall (1993) considered the effects of dust on the Lyα radiative transfer. Resonant scattering by atomic hydrogen significantly increases the path length for Lyα photons and consequently the likelihood of Lyα destruction by dust, leading to much lower line strengths. On cosmological scales, models incorporating a redshift-dependent intergalactic dust obscuration (Haiman & Spaans 1999; Malhotra & Rhoads 2004) predict Lyα space densities that are broadly consistent with "semi-analytical" models connecting Lyα emitting galaxies and dark matter halos.

Although there is consensus that Lyα is regulated by dust, no clear correlation has been found between dust content and Lyα EW at low redshift (z) (Giavalisco et al. 1996; Hansen & Oh 2006). However, at $z \sim 3$ the picture seems to be rather different. Shapley et al. (2003) found a significant correlation between UV continuum extinction and Lyα EW. They suggest that this difference between low and high redshift could be due to either differences in the geometry of dust in the neutral gas, or small sample statistics biases at low redshift. Furthermore, Laursen et al. (2013) found that different ISM morphologies are unlikely to account for different Lyα escape probabilities. Instead, they propose an increase of Lyα radiation due to cold accretion and/or anisotropic escape. Most importantly, the kinematic properties of the ISM may very well be the dominant escape or trapping mechanism for Lyα (Kunth et al. 2003; Fujita et al. 2003; Mas-Hesse et al. 2003; Dijkstra & Wyithe 2010).

In addition to physical processes related to the ISM, the observed Lyα emission can be modified by corrections for any underlying stellar Lyα. Depending on the stellar population properties, these corrections can be quite substantial and even cancel out the nebular emission. Valls-Gabaud (1993) suggested stellar Lyα absorption from an aged population as the reason for the dearth of Lyα emitters among local starburst galaxies.

The stellar Lyα cannot be fully constrained observationally since even the closest O stars in our Galaxy have ISM H I column densities high enough to produce strong interstellar Lyα, which masks their total intrinsic stellar line. In this work, we retrieved publicly available theoretical spectra of O and B stars generated with CMFGEN (Hillier & Miller 1998; Hillier 2012) and TLUSTY (Hubeny & Lanz 1995; Lanz & Hubeny 2003, 2007), respectively, and determined 276 individual Lyα EWs. The EWs are used as a library for implementation in the Starburst99 synthesis code (Leitherer et al. 1999; Leitherer & Chen 2009). The goal of our work is to predict the behavior of the stellar Lyα as a function of population properties. While understanding

the behavior of stellar Lyα is crucial in its own right, we are mainly motivated by the need to evaluate the effect of the stellar contribution to the total Lyα emission in star-forming galaxies. This work is organized as follows. In Section 2, we present a description of the models used for the new theoretical library, and we describe how we determined the EWs. In Section 3, we compare our determinations with observations of individual O and B stars, and in Section 4, we describe the implementation of the new library in the Starburst99 code and the resulting EWs of typical populations. In Section 5, we present our conclusions.

2. METHODOLOGY

Our goal is to predict the stellar Lyα line strength of a population of young stars whose ionizing photons give rise to the observed nebular Lyα emission. The relevant stars are of spectral types O and B. Later types contribute negligible light at 1216 Å in a population with OB stars present. Alternatively, a single, evolved population at an age older than ~100 Myr (when A stars start to dominate) would not be observed as a Lyα emitter because of the dearth of ionizing photons.

Strong stellar winds are a defining characteristic of OB stars. The spectral signatures of these winds are blueshifted absorption, broad emission, or P Cygni type profiles (Puls et al. 2008). Lyα in particular, is susceptible to wind effects due to its formation depth far above the photosphere. This was already recognized during the early efforts of non-local thermal equilibrium (non-LTE) modeling by Klein & Castor (1978), who emphasized that the strength of Lyα in luminous O stars is never significant due to canceling effects of the emission and absorption components.

In this work, we utilize stellar spectra of O stars computed with the CMFGEN atmosphere code, which was designed to solve the radiative transfer and statistical equilibrium equations in hot stars in spherical geometry (Hillier & Lanz 2001). The models account for non-LTE and are fully blanketed. The CMFGEN code was originally written for modeling the strong winds of Wolf–Rayet stars (Hillier 1987), but has since been generalized to be applicable to O stars as well. Pre-calculated grids of O-star models are readily available in various databases so that there is no need to generate additional models. We surveyed the available spectra of O stars from the Pollux database (Palacios et al. 2010), and retrieved 46 CMFGEN O-star spectra of solar metallicity, microturbulent velocity of 5 and 10 km s^{-1}, effective temperatures ($T_{\rm eff}$) ranging from 27,500 to 48,530 K, and surface gravity ($\log g$) ranging from 3.0 to 4.25. The mass-loss rate used in this O grid ranged from 4.85–8.34 $\times 10^{-6}$ $M_{\odot}$ yr^{-1}, and has been adopted to match the observed rates. A β-velocity law (Lamers & Cassinelli 1999) was adopted, with $\beta = 0.8$. The O grid available on the CMFGEN webpage[1] is a subset of that contained in the Pollux database and therefore provides no additional new data (the O grid in the CMFGEN Web site contains only 23 models of O stars).

Hot-star winds scale with luminosity and (to a smaller degree) with $T_{\rm eff}$ (Vink 2007). As a result, wind effects become less pronounced in B stars when compared to O stars. B-star spectra show less evidence for winds, except for the most luminous supergiants, which are rare by number in a typical stellar population. Given this situation, we opted for B-star models based on the TLUSTY atmosphere code (Lanz & Hubeny 2007). Like CMFGEN, TLUSTY is a fully metal-blanketed non-LTE code. In contrast to CMFGEN, TLUSTY adopts a static, plane-parallel geometry, which does not account for stellar-wind effects above the photosphere. TLUSTY is an excellent representation of B main-sequence stars and of evolved B stars with moderate winds. Modeled spectra of B stars were obtained from the TLUSTY Web site.[2] We used the BSTAR2006 grid of B stars with solar metallicity. We retrieved 212 modeled B star spectra with microturbulent velocities of 2 and 10 km s^{-1}, $T_{\rm eff}$ ranging from 15,000 to 30,000 K, and $\log g$ ranging from 1.75 to 4.75. The specific characteristics of the models are presented in Lanz & Hubeny.

Since winds are not completely absent in B-type stars, we need to be concerned about the applicability of the static TLUSTY models. Heap et al. (2006) provide an extensive discussion of the trades between the CMFGEN and TLUSTY codes. While the preference for spherical, expanding atmospheres in O stars is obvious, it is preferable to use sophisticated photospheric models such as TLUSTY for stars with moderate or weak winds rather than rely on spherical models with simplified physics of the deep, quasi-static layers. This justifies our choice of CMFGEN for O stars, and TLUSTY for B stars.

Massey et al. (2013) found that the choice of different microturbulent velocities has little effect on heavy element lines and no effect on the hydrogen lines. We measured the difference in the determined EWs from models with different microturbulent velocities. We found that the mode on this difference was ~3 Å, and the minimum and maximum differences were 0.1 and 7.2 Å, respectively. We used the microturbulence velocity of 10 km s^{-1} unless this value was not available. In Table 1, we give a summary of the models compiled for this work. There is a total of 258 model spectra considering all microturbulent velocities. The parameters cover the full observed range of $T_{\rm eff}$ and $\log g$ in the upper Hertzsprung–Russell diagram.

In order to obtain determinations of Lyα EWs[3] comparable to those obtained from observations, we rebinned the spectra from the extremely high resolution of the models ($\Delta\lambda$ of 0.060 Å for CMFGEN and 0.005 Å for TLUSTY at Lyα) to $\Delta\lambda$ of 0.465 Å. This was performed using a cubic spline function. This value is an average of $\Delta\lambda$ of 0.75 and 0.18 Å, the typical resolutions of the two spectrographs on board the *Hubble Space Telescope*, the Space Telescope Imaging Spectrograph and the Cosmic Origins Spectrograph, used for observing extragalactic objects.

Our determinations of EWs were performed with a simple flux over continuum integration code written in Python. For the TLUSTY modeled atmospheres, both the continuum and the line spectra were retrieved from their webpage. Hence, the EW determination was straightforward, since the continuum location is predefined. However, for the Pollux-retrieved spectral energy distributions, only the line spectra were available. As expected, the EW determination changed with the height at which the continuum was placed. The continuum was set to be a straight line between two points free of lines in a wavelength range from 1100 to 1300 Å. To test the validity of this method, we used the small grid of O stars from the CMFGEN Web site that do give both the continuum and the line files. We retrieved these files and normalized the spectra (divided the lines by the continuum files). We then determined the EWs with the Python code, integrating through 10 Å centered at Lyα. For the purpose of comparison, we will call these determinations the benchmark EWs. We then used only the line files to fit our straight line continuum method and

[1] http://kookaburra.phyast.pitt.edu/hillier/web/CMFGEN.htm

[2] http://nova.astro.umd.edu/index.html

[3] The sign convention used in this work is positive for emission lines and negative for absorption lines.

Table 1
Parameters of the Models Used for the New Library

$T_{\rm eff}$ (K)	log g	Code
15,000	1.75, 2.00, 2.25, 2.50, 2.75, 3.00, 3.25, 3.50, 3.75, 4.00, 4.25, 4.50	TLUSTY
16,000	2.00, 2.25, 2.50, 2.75, 3.00, 3.25, 3.50, 3.75, 4.00, 4.25, 4.50	TLUSTY
17,000	2.00, 2.25, 2.50, 2.75, 3.00, 3.25, 3.50, 3.75, 4.00, 4.25, 4.50	TLUSTY
18,000	2.00, 2.25, 2.50, 3.00, 3.25, 3.50, 3.75, 4.00, 4.25, 4.50	TLUSTY
19,000	2.25, 2.50, 2.75, 3.00, 3.25, 3.50, 3.75, 4.00, 4.25, 4.50	TLUSTY
20,000	2.25, 2.50, 2.75, 3.00, 3.25, 3.50, 3.75, 4.00, 4.25, 4.50	TLUSTY
21,000	2.50, 2.75, 3.00, 3.25, 3.50, 3.75, 4.00, 4.25, 4.50	TLUSTY
22,000	2.50, 2.75, 3.00, 3.25, 3.50, 3.75, 4.00, 4.25, 4.50	TLUSTY
23,000	2.50, 2.75, 3.00, 3.25, 3.50, 3.75, 4.00, 4.25, 4.50	TLUSTY
24,000	2.50, 2.75, 3.00, 3.25, 3.50, 3.75, 4.00, 4.25, 4.50	TLUSTY
25,000	2.50, 2.75, 3.00, 3.25, 3.50, 3.75, 4.00, 4.25, 4.50	TLUSTY
26,000	2.75, 3.00, 3.25, 3.50, 3.75, 4.00, 4.25, 4.50	TLUSTY
27,000	2.75, 3.00, 3.25, 3.50, 3.75, 4.00, 4.25, 4.50	TLUSTY
27,500	3.00, 3.75	CMFGEN
27,730	3.35	CMFGEN
28,000	2.75, 3.00, 3.25, 3.50, 3.75, 4.00, 4.25, 4.50	TLUSTY
29,000	3.00, 3.25, 3.50, 3.75, 4.00, 4.25, 4.50	TLUSTY
30,000	3.00, 3.25, 3.50, 3.75, 4.00, 4.25, 4.50	TLUSTY
30,000	3.00, 3.13, 3.50, 4.00, 4.10, 4.20	CMFGEN
30,270	3.29	CMFGEN
30,410	3.73	CMFGEN
31,480	4.06	CMFGEN
32,210	3.26	CMFGEN
32,500	3.25, 3.50, 3.60, 4.10, 4.25	CMFGEN
32,660	3.71	CMFGEN
33,340	4.01	CMFGEN
34,435	3.52	CMFGEN
35,000	3.25, 3.50, 4.10, 4.25	CMFGEN
36,310	4.02	CMFGEN
37,411	3.38	CMFGEN
37,500	3.50, 3.90	CMFGEN
37,670	3.77	CMFGEN
37,760	3.76	CMFGEN
39,540	3.68	CMFGEN
39,628	3.93	CMFGEN
39,994	3.63	CMFGEN
40,000	3.50, 3.90	CMFGEN
41,020	4.04	CMFGEN
41,591	3.80	CMFGEN
41,178	4.02	CMFGEN
42,560	3.71	CMFGEN
42,560	4.16	CMFGEN
43,954	3.98	CMFGEN
46,130	4.05	CMFGEN
48,530	4.01	CMFGEN

determined the EWs with the same Python code. The resulting EWs have on average an error of 1%, and up to 5% with respect to the benchmark EWs.

Figures 1 and 2 show representative spectra of O and B stars, respectively. In both figures the most prominent lines are marked for reference, and the red horizontal line indicates the position of the continuum and the EW integration range for each star type. These reference lines are C III 1175 Å, Si III 1206 Å, H I Lyα 1216 Å, N V 1240 Å, and C III 1247 Å. For O stars, the spectra of most models show clear P Cygni profiles, indicating the combination of photospheric absorption and high-density stellar winds due to radiation pressure (Leitherer et al. 1995). In the spectra of luminous O stars and even in the earliest B stars, the N V line can be quite prominent (and in some cases blend with Lyα), though its strength decreases for later B stars (Walborn et al. 1985). In turn, the Si III line does not play a major role in the spectra of O stars but in B stars this line can easily blend with Lyα, since the Lyα width increases considerably for later B-type stars (Walborn et al. 1995). Since in this study we aim to determine the stellar contribution of the observed Lyα EW, we want to avoid most of the possible blendings with Lyα. We therefore chose different EW integration ranges for O and B stars.

For the modeled O stars, the integration was performed over 10 Å centered on the rest-frame wavelength of the Lyα line (strictly 1215.67 Å). The EWs of these stars were average in absorption and mostly close to 0 Å due to the strong P Cygni wind profiles (see Figure 1). Hence, the chosen wavelength range of 10 Å allowed us to account for the full width of Lyα, including wings and the P Cygni profiles, if present.

For the modeled B stars, the integration was performed over 40 Å centered on the rest-frame wavelength of Lyα in order to

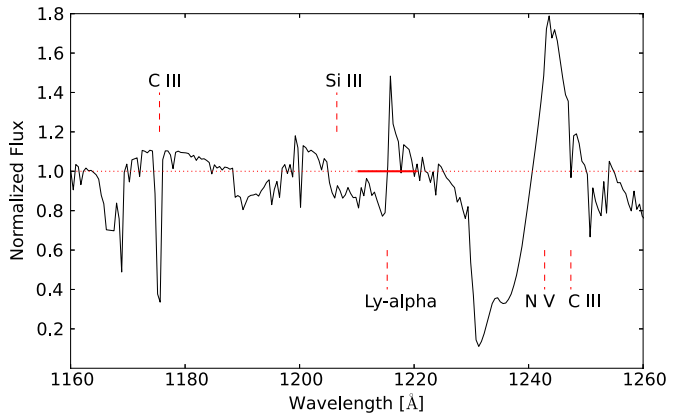

Figure 1. Theoretical spectrum of a CMFGEN O star with effective temperature of 40,000 K, log g of 3.5, and microturbulent velocity of 10 km s^{-1}. The red dashed vertical lines mark the rest wavelength of the most prominent lines. The red horizontal dotted and solid lines mark the continuum and integration window used for the "simple integration" method (see Section 2), respectively.

(A color version of this figure is available in the online journal.)

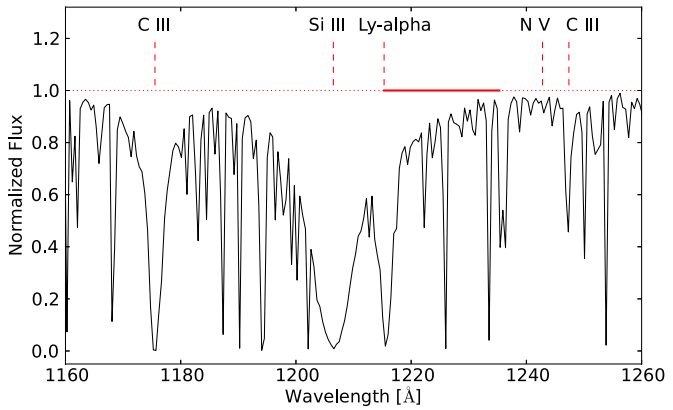

Figure 2. Theoretical spectrum of a TLUSTY B star with effective temperature of 18,000 K, log g of 4.25, and microturbulent velocity of 2 km s^{-1}. The red dashed vertical lines mark the rest wavelength of the most prominent lines. The red horizontal dotted and solid lines mark the continuum and integration window used for the "half integration" method (see Section 2), respectively.

(A color version of this figure is available in the online journal.)

account for the broader Lyα absorption. For clarity, we will call this determination the "simple integration" EW. Nonetheless, the Si III resonance line at 1206.5 Å is an important source of line blending for B stars (Savage & Panek 1974). In order to correct for the contribution of this line to Lyα we assumed that Lyα was symmetric, and avoided the part of the spectrum where Si III and Lyα overlap. We integrated the EW from the rest wavelength of Lyα to Lyα+20 Å and then multiplied this EW by 2. We call this determination the "half integration" EW.

Savage & Panek (1974) found that the typical contribution of the Si III line to Lyα is about 4 Å. When comparing the Lyα EW determinations through the "simple integration" EW to the "half integration" EW, we found that the difference between the first and the second EW determination is on average 3 Å but peaks between log g of 2.0 and 2.50 to about 7 Å below an effective temperature of 21,000 K. We chose the "half integration" EW to better represent the Lyα EW since the Si III line is a clear systematic feature in the modeled B-star spectra (see Figure 2). The resulting EW determinations for B stars are all in absorption and range from 1 to 32.5 Å.

For $T_{\rm eff}$ of 15,000 to 30,000 K we used the TLUSTY models and for $T_{\rm eff} > 30{,}000$ K we used the CMFGEN models. We did a linear interpolation to obtain the EWs for those values of $T_{\rm eff}$ and

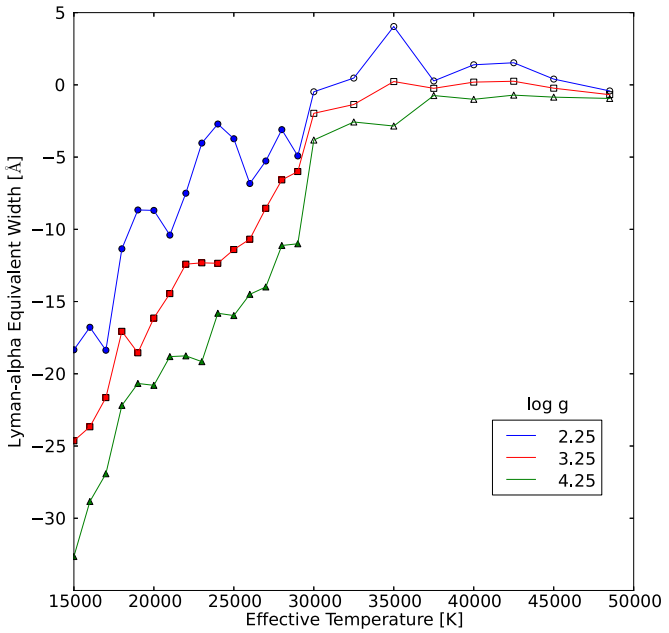

Figure 3. Plot of Lyα EW vs. effective temperature. Three representative curves are presented. The top curve (blue circles) represents the Lyα EW for stars with a log g of 2.25, the middle curve (red squares) for stars with a log g of 3.25, and the lower curve (green triangles) for stars with log g of 4.25. Filled symbols represent TLUSTY stars, while open symbols represent CMFGEN stars.

(A color version of this figure is available in the online journal.)

log g that were not included in the model spectra we retrieved. The final EWs adopted in this work are presented in Table 2. Figure 3 shows the trend of our EW determinations with respect to $T_{\rm eff}$ for different values of log g. We attribute the slight jump in this figure to the different treatments of the stellar winds used in TLUSTY and CMFGEN codes. Nonetheless, in order to check for consistency between both codes, we studied the differences between EW measurements in the overlapping region (i.e., $T_{\rm eff}$ between 27,000 and 30,000 K). We found that the mode and average difference of the CMFGEN and the TLUSTY EWs is about 7 Å, with a maximum difference of 9 Å at $T_{\rm eff}$ of 30,000 K and log g of 3.75.

The behavior shown in Figure 3 is consistent with what is expected from the observations. For both O and B stars, the intensity and width of the ultraviolet features is closely related to the luminosity type (Walborn et al. 1995). Spectra of O stars show a P Cygni profile in some lines (late-B stars for metal lines) when the absorbing ion column density is larger than about 10^{15} ions cm^{-2} (Lamers & Cassinelli 1999). This is precisely the overlapping region in our EW measurements, from 27,000 to 30,000 K. The P Cygni profiles for Lyα become progressively smaller as $T_{\rm eff}$ decreases, hence making the EW progressively differ from zero (i.e., a greater absorption as the wind emission becomes smaller). As $T_{\rm eff}$ keeps decreasing, the Lyα absorption becomes wider.

In order to explore how non-solar chemical compositions affect the Lyα EW, we obtained spectra of TLUSTY of B stars with $T_{\rm eff}$ of 30,000 K and log g of 4.25, and with four different metallicities besides solar. These stars are also described in Lanz & Hubeny (2007). We determined the EWs with the "half integration" method. The determined Lyα EWs for metallicities (in units of $Z/Z_{\odot}$) of 2, 1, 1/2, 1/5, and 1/10 were -15.38, -12.87, -10.43, -9.85, and -6.30 Å, respectively. The overall shape of the spectrum changes very little with metallicity, i.e., the lines around Lyα become less prominent, making it easier to

Table 2
Lyα Equivalent Widths[a] as a Function of Effective Temperature and log *g*

$T_{\rm eff}$	Lyα EW (Å) for log *g* of:											
(K)	1.75	2.00	2.25	2.50	2.75	3.00	3.25	3.50	3.75	4.00	4.25	4.50
15,000	−15.3	−20.6	−18.3	−22.6	−25.5	−25.6	−24.6	−27.9	−29.3	−29.3	−32.6	−32.5
16,000	−12.2	−13.8	−16.8	−17.8	−19.8	−20.8	−23.7	−24.2	−25.0	−27.5	28.8	−29.7
17,000	−9.6	−11.1	−18.4	−16.0	−16.6	−19.7	−21.7	−21.7	−23.8	−24.6	−26.9	−25.9
18,000	−3.8	−5.7	−11.4	−13.6	−15.5	−15.4	−17.1	−19.4	−20.3	−24.4	−22.2	−24.3
19,000	−5.2	−7.0	−8.7	−9.4	−15.7	−14.3	−18.5	−18.6	−20.6	−19.8	−20.7	−24.1
20,000	−5.8	−7.2	−8.7	−11.5	−13.6	−13.6	−16.1	−15.5	−18.01	−17.9	−20.8	−21.7
21,000	−8.1	−9.2	−10.4	−11.6	−10.8	−12.5	−14.5	−14.4	−16.9	−17.9	−18.8	−20.9
22,000	−5.0	−6.3	−7.5	−8.7	−10.6	−12.2	−12.4	−14.9	−15.2	−16.9	−18.8	−18.6
23,000	−1.3	−2.7	−4.0	−5.4	−10.9	−11.0	−12.3	−12.2	−14.8	−14.3	−19.2	−16.2
24,000	0.9	−0.9	−2.7	−4.5	−9.0	−10.0	−12.4	−13.5	−15.7	−17.0	−15.8	−18.8
25,000	−0.7	−2.2	−3.7	−5.3	−6.8	−11.2	−11.4	−11.9	−12.7	−16.3	−16.0	−17.5
26,000	−4.8	−5.8	−6.8	−7.8	−8.8	−9.6	−10.6	−10.7	−14.1	−12.9	−14.5	15.9
27,000	−3.5	−4.4	−5.3	−6.2	−7.0	−10.4	−8.5	−10.0	−12.2	−11.8	−14.0	−13.2
28,000	−1.0	−2.0	−3.1	−4.2	−5.2	−7.5	−6.6	−8.1	−11.2	−12.8	−11.1	−12.7
29,000	−3.5	−4.2	−4.9	−5.6	−6.3	−7.0	−6.0	−8.0	−11.0	−12.0	−11.0	−11.2
30,000	0.4	−0.1	−0.5	−0.9	−1.3	−1.7	−2.0	−2.6	−3.0	−3.4	−3.8	−4.3
32,500	1.5	1.0	0.5	−0.0	−0.5	−1.1	−1.4	−2.1	−2.4	−3.1	−2.6	−4.1
35,000	5.9	5.0	4.0	3.1	2.1	1.2	0.2	−1.3	−1.7	−2.6	−2.8	−4.5
37,500	0.5	0.4	0.3	0.1	0.0	−0.1	−0.2	−0.4	−0.5	−0.6	−0.7	−0.9
40,000	2.0	1.7	1.4	1.1	0.8	0.5	0.2	−0.1	−0.4	−0.7	−1.0	−1.3
42,500	2.2	1.8	1.5	1.2	0.9	0.5	0.3	−0.1	−0.4	−0.7	−1.0	−1.4
45,000	0.7	0.6	0.4	0.2	0.1	−0.1	−0.2	−0.4	−0.5	−0.7	−0.9	−1.0
48,500	−0.3	−0.4	−0.4	−0.5	−0.6	−0.6	−0.7	−0.7	−0.8	−0.9	−0.9	−1.0

Note. [a] The sign convention used for this work is positive for emission and negative for absorption.

detect Lyα even considering that the EW is also getting smaller. This behavior is as expected since (1) the EW is defined as the wavelength range over which the continuum around the line must be integrated to produce the same intensity as the observed line (Lallement et al. 2011), and (2) the effect of metallicity on other hydrogen lines such as the Balmer lines is also rather weak if $T_{\rm eff}$ is higher than 7000 K (González-Delgado & Leitherer 1999).

3. COMPARISON WITH OBSERVATIONS OF O AND B STARS

In order to gain confidence into our set of Lyα EWs, we surveyed the literature for available observations of stellar Lyα. There is a rich body of data dating back to the early observations by OAO-2 (Savage & Jenkins 1972), OAO-3 (Bohlin et al. 1978), and IUE (Diplas & Savage 1994a, 1994b). We compared our theoretical Lyα EW determinations with those from observations of O and B stars presented in Savage & Code (1970) and Savage & Panek (1974). The observations presented in Savage & Code and Savage & Panek were taken with OAO-2, whose spectrograph had a resolution of 15 Å. The relatively low resolution implies that there could be contamination with Si III on the short-wavelength side of Lyα and possibly with N V on the long-wavelength side, depending on the extent of the wings of Lyα.

We adopted the EWs as published by Savage & Code (1970) and Savage & Panek (1974), with the sign convention used throughout this work. Contamination of stellar Lyα by the interstellar H I absorption is a serious concern, in particular for O stars whose larger average distances (when compared to B stars) lead to interstellar neutral hydrogen column densities $N_{\rm H}$ in excess of 10^{20} cm^{-2}. As a result, the measured Lyα EWs in essentially all O stars are not stellar but interstellar. Since the derived lower limits of the stellar contribution to the total Lyα would provide little insight into the validity of our models, we did not consider stars with $T_{\rm eff} > 35{,}000$ K for our comparison. This cut-off corresponds to spectral type O9. In Table 3, we present the selected stars together with the pertinent parameters. Columns 1 and 2 list the designations. The spectral types are in column 3. $T_{\rm eff}$ (column 4) was assigned using the calibration of Conti et al. (2008). Observed EW values are in column 5.

In Figure 4, we show the comparison between the observed and theoretical EW values as a function of stellar effective temperature. The models display a near-monotonic trend with $T_{\rm eff}$, asymptotically reaching about zero Å at $T_{\rm eff} > 35{,}000$ K. At a given $T_{\rm eff}$, a larger log *g* results in stronger Lyα absorption. The observed values track the models very well at the lowest temperatures but tend to be more negative (stronger absorption) at higher temperatures (corresponding to early B stars). We interpret this as not due to a model failure but rather being caused by residual interstellar contamination. In support of this suggestion we indicated the measured $E(B-V)$ values for each observation, taken from Savage & Code (1970) and Savage & Panek (1974). There is a clear trend of the largest discrepancies between models and data occurring for the highest $E(B-V)$ values. Since there is a well-established relation between $E(B-V)$ and interstellar $E(B-V)$ (Diplas & Savage 1994a), we conclude that the majority of the observational points below the models are in fact just lower limits to the stellar contribution.

The outcome of the comparison between the modeled and observed EWs is quite reassuring. While there are few observational constraints on the Lyα EWs in O stars, the intrinsic Lyα in the hottest stars is expected to be weak because of the counteracting effects of photospheric absorption and wind emission. Therefore, these stars would make only a minor contribution to the total stellar absorption in a representative population. B stars, on the other hand, when present in a population, can contribute

Table 3
Lyα Equivalent Width Measurements from Observations[a] as a Function of Effective Temperature

Star (HD Number)	Name	Spectral Type	Lyα EW (Å)	$T_{\rm eff}$ (K)
	Taken from Savage & Code (1970)[b]			
11415[c]	ϵ Cas	B3 IVp	−28	17,500
24398	ζ Per	B1 Ib	−25	21,500
24760	ϵ Per	B0.5 V	−14	28,000
29763	τ Tau	B3 V	−29	17,500
32630[c]	η Au	B3 V	−25	17,500
34816	λ Lep	B0.5 IV	−14	27,500
35411	η Ori	B0.5 V	−20	28,000
35439	25 Ori	B1 Vpe	−19	26,000
35468	γ Ori	B2 III	−15	19,750
35497[c]	β Tau	B7 III	−35	12,700
36485-86	δ Ori	O9.5 II	−20	29,625
36512	ν Ori	B0 V	−13	29,500
36822	ϕ' Ori	B0 IV	−31	29,000
37022	41 Ori	O7 V		37,000
−41	θ Ori	O9.5 Vp	−33	31,500
37043	ι Ori	O9 III	−17	32,250
37128	ϵ Ori	B0 Ia	−24	27,500
37202	ζ Tau	B2 IVp	−21	20,375
37468	σ Ori	O9.5 V	−16	31,500
37742-43	ζ Ori	O9.5 Ib	−25	29,000
38771	κ Ori	B0.5 Ia	−22	26,000
44743	β CMa	B1 II	−10	22,625
52089	ϵ CMa	B2 II	−12	19,125
87901[c]	α Leo	B7 V	−43	13,300
116658	α Vir	B1 V	−11	26,000
120315[c]	η Uma	B3 V	−22	17,500
122451	β Cen	B1 II	−12	22,625
127381	σ Lup	B2 V	−20	21,000
127972	η Cen	B1.5 Vne	−15	24,000
128345[c]	ρ Lup	B5 V	−36	15,400
129056	α Lup	B1 V	−14	26,000
132200	κ Cen	B2 V	−17	21,000
133242-43[c]	π Lup	B5 IV	−26	14,925
133955[c]	λ Lup	B3 V	−22	17,500
136298	δ Lup	B2 IV	−14	20,375
136664	ϕ^2 Lup	B5 V	−26	15,400
139365[c]	τ Lib	B2.5 V	−22	19,000
141637	1 Sco	B2.5 Vn	−30	19,000
142983	48 Lib	B8 Ia/Iab	−12	11,400
143018	π Sco	B1 V	−18	26,000
143275	δ Sco	B0 V	−24	29,500
144470	ω^1 Sco	B1 V	−33	26,000
147165	σ Sco	B1 III	−31	23,750
149757	ζ Oph	O9.5 V	−26	31,500
151890	μ' Sco	B1.5 V	−20	24,000
158926	λ' Sco	B1 V	−12	26,000
160578	κ Sco	B2 IV	−16	20,375
189103	Θ′ Sgr	B3 IV	−29	17,000
209952[c]	α Gru	B5 V	−33	15,400
	Taken from Savage & Panek (1974)[d]			
358	α And	B9 II	−45	10,850
10144	α Eri	B3 Vp	−21	17,500
11415[c]	ϵ Cas	B3 Vp	−25	17,500
19356	β Per	B8 V	−65	12,300
22928	δ Per	B5 III	−31	14,450
32630[c]	η Aur	B3 V	−22	17,500
34085	β Ori	B8 Ia	>−30	11,400
35497[c]	β Tau	B7 III	−42	12,700
37795	α Col	B7 IV	−45	13,000
42560	ξ Ori	B3 IV	−21	17,000
44402	ζ CMa	B2.5 IV	−20	18,375
6575	χ Car	B3 IVp	−19	17,000
87901[c]	α Leo	B7 V	−55	13,300
120315[c]	η UMa	B3 V	−25	17,500
121263	ζ Cen	B2.5 IV	−10	18,375
125238	ι Lup	B2.5 IV	−18	18,375
125823	α Cen	B7 IIIp	−23	12,700
128345[c]	ρ Lup	B5 V	−45	15,400
129116		B3 V	−20	17,500
133242[c]	π Lup	B5 V	−30	15,400
−43[d]		B5 IV		14,975
133955[c]	λ Lup	B3 V	−21	17,500
139365[c]	τ Lib	B2.5 V	−19	19,000
143118	η Lup	B2.5 IV	−11	18,375
147394	τ Her	B5 IV	−35	14,925
155763	ζ Dra	B6 III	−44	13,600
160762	ι Her	B3 IV	−21	17,000
175191	σ Sgr	B3 IV	−18	17,000
193924	α Pav	B2.5 V	−17	19,000
209952[c]	α Gru	B7 IV	−45	13,000

Notes.
[a] The signs of the measured EWs were changed from the original papers in order to maintain the convention of this work; absorption is represented by a negative EW.
[b] The EWs in this table include the blending with neighboring lines within 15 Å (the OAO resolution), and also the blend with the interstellar Lyα line.
[c] These stars are present in both papers, Savage & Code (1970) and Savage & Panek (1974).
[d] The Savage & Panek (1974) EWs in this table were those corrected for interstellar absorption and for the blend with neighboring lines.

substantially, and their modeled Lyα is in very good agreement with the data.

4. POPULATION SYNTHESIS MODELS

The Lyα EWs listed in Table 2 were implemented in the synthesis code Starburst99 (Leitherer et al. 1999; Leitherer & Chen 2009). We performed a two-dimensional interpolation in $T_{\rm eff}$ and $\log g$ to obtain the EW values for each point in the Hertzsprung-Russell diagram as prescribed by the stellar evolutionary tracks. The input table is essentially complete at the highest temperatures, and no significant extrapolations were required. For $T_{\rm eff}$ between 15,000 K and 10,000 K (late B stars), we used Equation (1) of Valls-Gabaud (1993) to approximate the Lyα EW. No attempt was made to account for EW at even lower $T_{\rm eff}$, and we simply assumed a featureless continuum for $T_{\rm eff} < 10{,}000$ K. This means our models are no longer valid when A stars begin to contribute to the UV continuum. We do not distinguish between O and Wolf–Rayet stars when assigning Lyα EWs to stars in the Hertzsprung–Russell diagram. The underlying assumption is that Lyα (or the He II line at approximately the same wavelength) in Wolf–Rayet stars behaves in a similar fashion as in hot O stars.

The nebular Lyα was calculated assuming standard Case B recombination for an electron temperature of 10^4 K. For reference, the Lyα/Hα ratio is 8.7 under these assumptions (Case A would be 11.4).

We created a standard set of synthetic Lyα EWs for evolving stellar populations using the Geneva evolution models with high

Table 4
Comparison of Lyα Equivalent Widths[a]

Authors	Stellar Component EW (Å)		Nebular Component EW (Å)		Total EW (Å) = stellar + nebular	
	5×10^6 yr	15×10^6 yr	5×10^6 years	15×10^6 yr	5×10^6 yr	15×10^6 yr
Instantaneous SFR						
This work	−8	−17	40	1	32	−16
Charlot & Fall (1993)	...	...	...	...	210	53
Valls-Gabaud (1993)	−5	−15	205	5	200	−10
Schaerer & Verhamme (2008)	−4	−20	47	3	43	−17
Constant SFR						
This work	−4	−7	145	100	141	93
Charlot & Fall (1993)	...	...	...	...	217	110
Valls-Gabaud (1993)	−3	−5	253	195	250	190
Schaerer & Verhamme (2008)	−1	−4	131	80	130	76

Notes. These values were determined for a Salpeter IMF, a stellar population with ages 5×10^6 and 15×10^6 yr, and solar metallicity.
[a] The sign convention used for this work is positive for emission and negative for absorption.

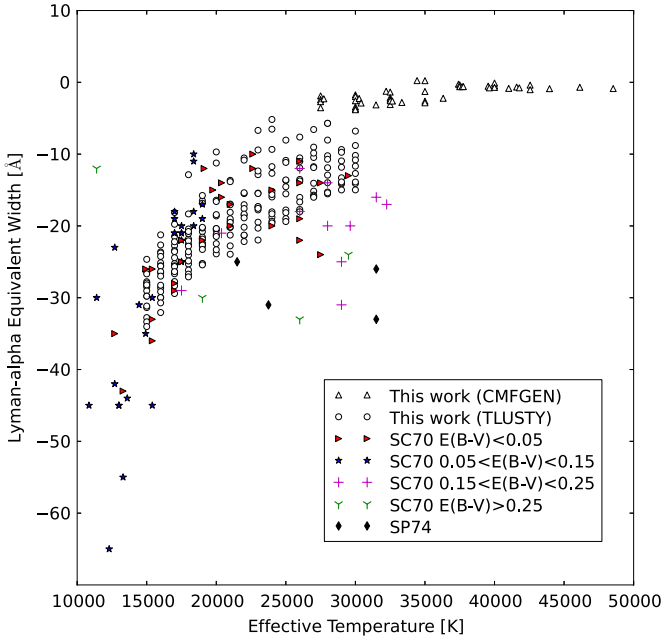

Figure 4. Comparison between our Lyα EW determinations and those from observations, as a function of effective temperature. Symbols represent the following: open up triangles are EW determinations of this work from CMFGEN models, open circles are EW determinations from TLUSTY models, red rotated triangles, magenta crosses, black diamonds, and green three-pointed stars are EWs obtained from observations from Savage & Code (1970), SC70, for different values of $E(B-V)$, and blue stars are EWs obtained from observations from Savage & Panek (1974), SP74. SC70 measurements are blended with the interstellar Lyα line and with neighboring lines, and SP74 are corrected for both ISM and blending with the Si III.

(A color version of this figure is available in the online journal.)

mass loss at solar chemical composition (Meynet et al. 1994). As a consistency check, we compared our predictions with those published in the literature. A standard Salpeter IMF has been adopted for these comparisons. Charlot & Fall (1993) and Valls-Gabaud (1993) were the first to draw attention to the importance of underlying stellar Lyα for the interpretation of nebular Lyα in star-forming galaxies. They both used the original Bruzual & Charlot (1993) evolutionary synthesis models with a correction of stellar Lyα to predict the net nebular + stellar Lyα. The stars evolve along the tracks computed by Maeder & Meynet (1989) in these models. In Table 4, we compare their and our predictions for selected ages and for the two limiting cases of an instantaneous burst and continuous star formation. Also included in Table 4 are the predictions of Schaerer & Verhamme (2008), who used a modified version of the Schaerer (2003) evolutionary synthesis models for predictions of nebular + stellar Lyα. The different sets of models are in reasonable agreement. The differences reflect the use of different evolutionary tracks and different model atmospheres. Note in particular that the larger EW at age 5×10^6 yr in the Charlot & Fall and Valls-Gabaud models is the result of different lifetimes in the stellar evolution models. At this age, the nebular Lyα displays a sharp drop with age, and a slight shift in age causes a vastly different ionizing photon output.

We performed a parameter study in order to analyze the impact of different IMFs, different ages, and different star formation histories in the Lyα EWs. The two bracketing cases of an instantaneous burst and constant star formation were considered. Starburst99 assumes a power-law IMF of the classical form $\phi(m) \propto m^{-\alpha}$. In this notation, the classical Salpeter IMF has an exponent of $\alpha = 2.35$. In Figures 5 and 6 we show the resulting Lyα EWs for different IMF slopes in the case of an instantaneous burst and continuous star formation, respectively.

We first address the relative importance of the underlying stellar Lyα at different ages in each of the two cases. The burst models (Figure 5) fall into two regimes: at young ages ($t \lesssim 6$ Myr), the nebular part always dominates since copious O-star photons are available and O stars have intrinsically weak Lyα. At older ages ($t \gtrsim 10$ Myr), the starburst is B-star dominated with few ionizing photons but at the same time intrinsically strong stellar Lyα. In the case of continuous star formation (Figure 6), the nebular component always dominates, and the underlying stellar Lyα is always negligible. As a reminder, this assumes pure Case B recombination for the nebular Lyα with a 100% photon escape.

Different IMF exponents, ranging from an extreme, flat IMF of $\alpha = 0.5$ to another extreme, steep value of $\alpha = 2.6$, only have a minor influence on the *stellar* Lyα EWs. The EW varies by about 2 Å for the considered IMF exponents between 0.5 and 2.6 for an instantaneous burst. This is expected for a single population where the stellar flux at a particular wavelength comes from stars over a very narrow mass range. In the continuous case, the IMF sensitivity of the stellar Lyα is somewhat more pronounced but still quite minor.

Next, we turn to the IMF dependence of the *nebular* component of Lyα. The IMF has a much more pronounced effect in this case, which can easily be understood from the fact the

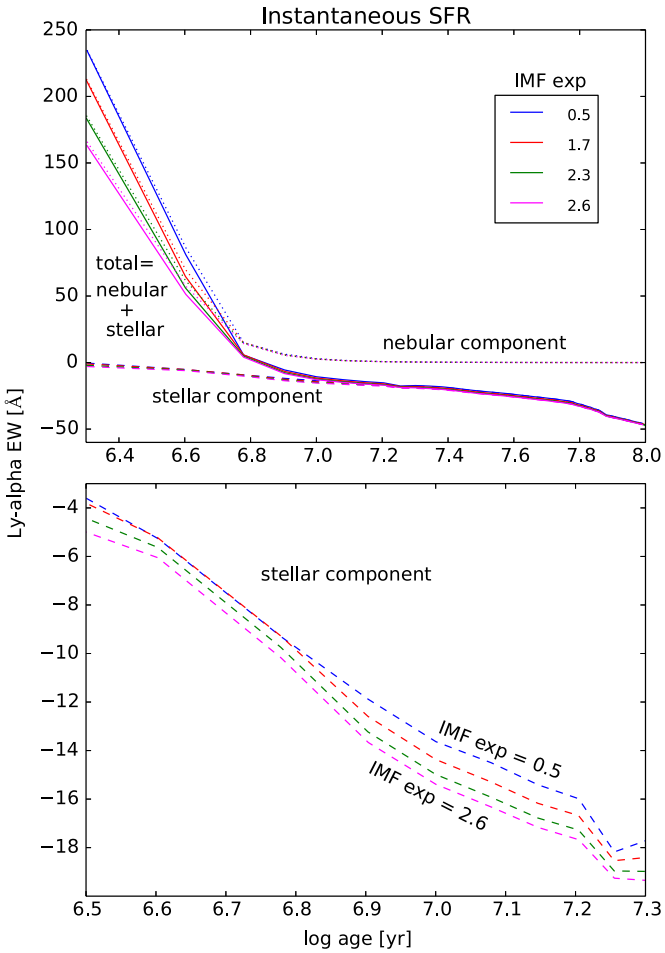

Figure 5. Lyα EWs vs. age for an instantaneous burst. This figure shows a series of Starburst99 runs for different IMF exponents, labeled by color from 0.5 (blue) through 2.6 (magenta). Salpeter is represented by the green curve. Dashed lines represent the stellar component of Lyα EWs, dotted lines represent the nebular component, and solid lines the total component. The sign convention used for this work is positive for emission and negative for absorption. The upper panel shows the overall behavior of Lyα up to 100 million years. The bottom panel shows a zoom-in of the stellar component from about 3 to 20 million years.

(A color version of this figure is available in the online journal.)

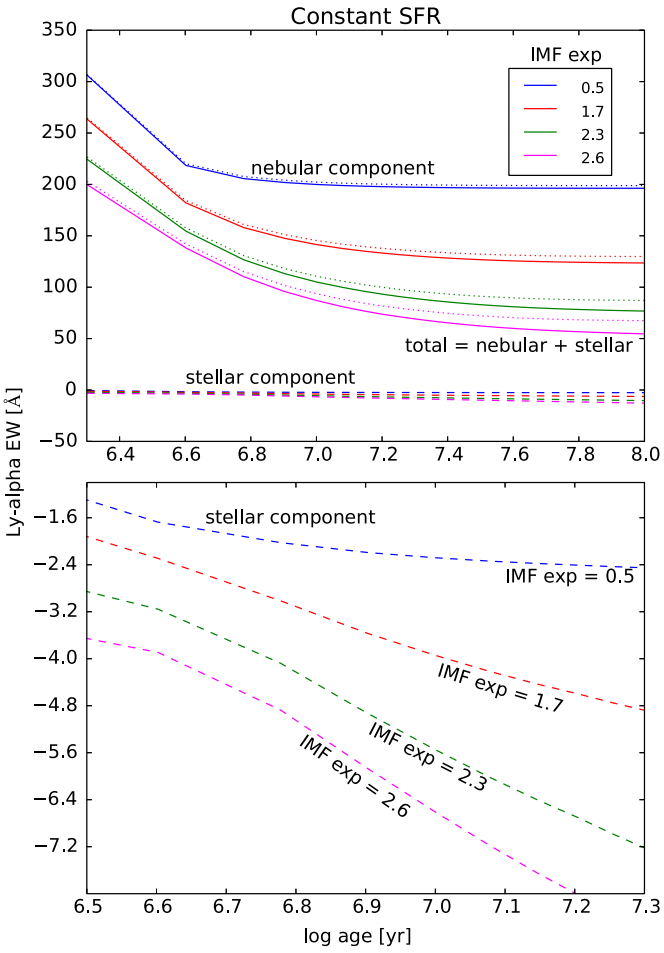

Figure 6. Same as Figure 5 but for constant star formation rate.

(A color version of this figure is available in the online journal.)

EW(Lyα) is determined by the ratio of early- to late-O stars, which contribute the ionizing photons and the continuum. Varying the IMF slope will change the relative contributions of these species. Therefore, the IMF behavior in Figures 5 and 6 is not surprising and mirrors that of, e.g., the Hα or Hβ EW, which has been extensively discussed in the literature (Leitherer et al. 1999).

The previous discussion is based on the assumption of a 100% escape probability of the nebular Lyα photons. Observations suggest a much lower escape fraction. For instance, the Lyα EWs observed in Lyman-break galaxies at redshift ∼3 are of the order of 10 Å (Shapley et al. 2003). Comparison with our continuous models uncorrected for stellar absorption, implies an escape of Lyα photons of ∼10%. In order to provide a more realistic model grid for comparison with the data, we generated models with a Salpeter IMF and nebular Lyα escape fractions of 5%, 10%, 25%, 50%, and 100%. These models are plotted in Figures 7 and 8 for instantaneous bursts and continuous star formation, respectively. Because of the reduced nebular emission for escape fractions less than 100%, the underlying stellar absorption drastically increases in its contribution to the

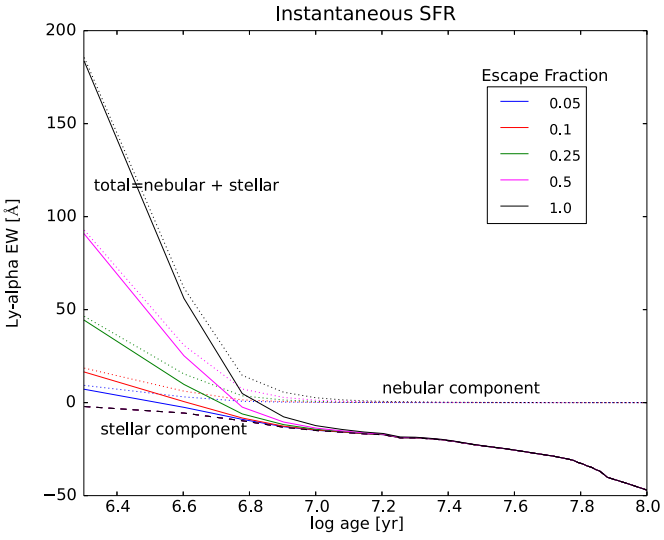

Figure 7. Lyα EWs vs. age for an instantaneous burst for different Lyα escape fractions. This figure shows a series of Starburst99 runs for an IMF exponent of 2.3. Dashed lines represent the stellar component of Lyα EWs, dotted lines represent the nebular component, and solid lines the total component. The sign convention used for this work is positive for emission and negative for absorption.

(A color version of this figure is available in the online journal.)

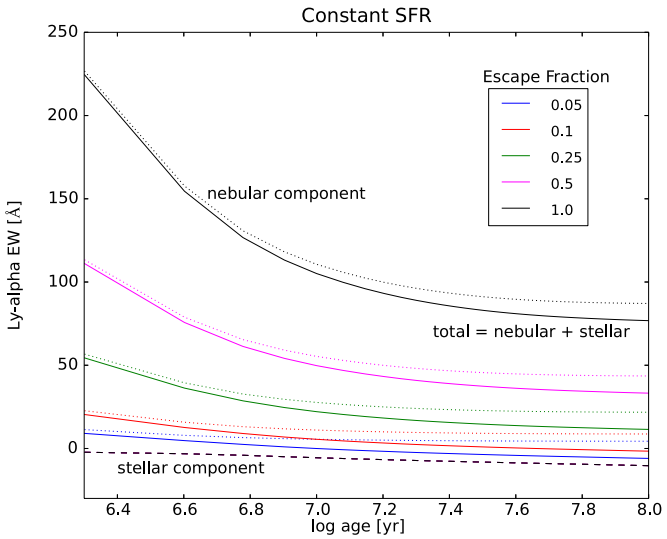

Figure 8. Same as Figure 7 but for constant star formation rate.
(A color version of this figure is available in the online journal.)

net EW. For instance, if the escape fraction is 10%, the stellar absorption and nebular emission EWs become comparable for continuous star formation at ages of 10–20 Myr.

5. CONCLUSIONS

We present a grid of theoretical stellar Lyα EWs for evolving stellar populations. While these models have value in their own right, our main motivation for presenting the grid is the need to correct nebular Lyα emission in star-forming galaxies for underlying stellar absorption. This study builds on the pioneering work of Valls-Gabaud (1993) and Charlot & Fall (1993) who had to rely on earlier, less complete model atmospheres, and it extends the exploratory work of Schaerer & Verhamme (2008), who used the latest model atmospheres for a restricted parameter range.

We compiled a new library of non-LTE Lyα EWs based on fully line-blanketed models. The library includes O and B stars with effective temperatures ranging from 15,000 K to 48,500 K, and log g from 1.75 to 4.5. The measured Lyα EWs range from 5.9 to -32.5 Å. In particular, we obtained Lyα EWs between 0.9 and -32.5 Å for effective temperatures of 15,000 K to 29,000 K, and values mostly close to 0 Å for higher effective temperatures due to the canceling effects of the emission and absorption of the P Cygni profiles of these stars. Metallicity has very little effect on the Lyα EWs.

We implemented the library in Starburst99 and studied the behavior of the Lyα EW for a range of stellar population properties. We performed a parameter study of instantaneous and continuous star formation at solar metallicity, using the high-mass-loss Geneva evolution models (Meynet et al. 1994). We found that (1) the IMF has only a minor influence on the *stellar* EW when varied within astrophysically plausible limits for both an instantaneous and a constant star formation rate (SFR). (2) The IMF also has a minor influence on the nebular component of the Lyα EW for an instantaneous SFR; however, for a continuous SFR, the difference between the two extreme IMF exponents (0.5 and 2.6) in the nebular component of the Lyα EW is about 100 Å at 3 Myr and about 180 Å at 15 Myr. (3) When O stars dominate the spectrum (as indicated by the presence of nebular emission lines), stellar Lyα absorption is always small compared to gaseous Lyα (if nebular Lyα has an escape fraction close to 100%). (4) Depending on the escape fraction of nebular Lyα photons, the stellar contribution to the total ranges from negligible to dominant. If the nebular escape fraction is 10%, the stellar absorption and nebular emission EWs become comparable for continuous star formation at ages of 10–20 Myr.

In stark contrast to the often used stellar absorption correction of 50–240 Å, our models predict (1) stellar Lyα EW values of 9–18 Å in absorption for an instantaneous burst between the ages of 5 and 15 Myr, and (2) values of 2–8 Å also in absorption for constant star formation in the same age range. Our models provide a realistic description of the stellar Lyα and should be appropriate to correct the nebular emission for underlying stellar absorption in star-forming galaxies.

We are grateful to an anonymous referee for a careful reading of the manuscript and many useful suggestions. We are also grateful to John Hillier for kindly providing us with plane-parallel CMFGEN models to check consistency between the results of CMFGEN and TLUSTY modeled atmospheres. Support for this work has been provided by NASA through grant number N-1317 from the Space Telescope Science Institute, which is operated by AURA, Inc., under NASA contract NAS5-26555.

REFERENCES

Bohlin, R. C., Savage, B. D., & Drake, J. F. 1978, ApJ, 224, 132
Bromm, V., & Yoshida, N. 2011, A&A, 49, 373
Bruzual, G., & Charlot, S. 1993, ApJ, 405, 538
Charlot, S., & Fall, M. 1993, ApJ, 415, 580
Conti, P. S., Crowther, P. A., & Leitherer, C. 2008, From Luminous Hot Stars to Starburst Galaxies (Cambridge: Cambridge Univ. Press)
Dijkstra, M., & Wyithe, S. B. 2010, MNRAS, 408, 352
Dijkstra, M., & Wyithe, S. B. 2012, MNRAS, 419, 3181
Diplas, A., & Savage, B. 1994a, ApJ, 427, 274
Diplas, A., & Savage, B. 1994b, ApJS, 93, 211
Fujita, S. S., Ajiki, M., Shioya, Y., et al. 2003, AJ, 125, 13
Giavalisco, M., Koratkar, A., & Calzetti, D. 1996, ApJ, 446, 831
González-Delgado, R. M., & Leitherer, C. 1999, ApJ, 125, 479
Haiman, Z., & Spaans, M. 1999, in AIP Conf. Proc. 470, The 9th Astrophysics Conference: After the Dark Ages, When Galaxies Were Young (the Universe at 2<Z<5), ed. S. S. Holt & E. P. Smith (Melville, NY: AIP), 63
Hansen, M., & Oh, S. P. 2006, MNRAS, 367, 979
Hartmann, L. W., Huchra, J. P., Geller, M. J., O'Brien, P., & Wilson, R. 1988, ApJ, 326, 101
Heap, S. R., Lanz, T., & Hubeny, I. 2006, ApJ, 638, 409
Hillier, D. J. 1987, ApJS, 63, 947
Hillier, D. J. 2012, in IAU Symp. 282, From Interacting Binaries to Exoplanets: Essential Modeling Tools, ed. M. T. Richards & I. Hubeny (Cambridge: Cambridge Univ. Press), 229
Hillier, D. J., & Lanz, T. 2001, in ASP Conf. Ser. 247, Spectroscopic Challenges of Photoionized Plasmas, ed. G. Ferland & D. W. Savin (San Francisco, CA: ASP), 343
Hillier, D. J., & Miller, D. L. 1998, ApJ, 496, 407
Hubeny, I., & Lanz, T. 1995, AJ, 439, 875
Kennicutt, R. C., & Evans, N. J. 2012, ARA&A, 50, 531
Klein, R. I., & Castor, J. I. 1978, ApJ, 220, 902
Kunth, D., Leitherer, C., Mas-Hesse, J. M., Östlin, G., & Petrosian, A. 2003, ApJ, 597, 263
Lallement, R., Quémarais, E., Bertaux, J. L., et al. 2011, Sci, 334, 1665
Lamers, H. J. G. L. M., & Cassinelli, J. P. (ed.) 1999, Introduction to Stellar Winds (Cambridge: Cambridge Univ. Press)
Lanz, T., & Hubeny, I. 2003, ApJS, 147, 225
Lanz, T., & Hubeny, I. 2007, ApJS, 169, 83
Laursen, P., Duval, F., & Östlin, G. 2013, ApJ, 766, 124
Leitherer, C., & Chen, J. 2009, NewA, 4, 356
Leitherer, C., Ortiz, P., Bresolin, F., et al. 2010, ApJS, 189, 309
Leitherer, C., Robert, C., & Heckman, T. M. 1995, ApJS, 99, 173
Leitherer, C., Schaerer, D., Goldader, J., et al. 1999, ApJS, 123, 3
Maeder, A., & Meynet, G. 1989, A&A, 210, 155
Malhotra, S., & Rhoads, J. 2002, ApJL, 565, L71

Malhotra, S., & Rhoads, J. 2004, ApJL, 617, L5
Mas-Hesse, J. M., Kunth, D., Tenorio-Tagle, G., et al. 2003, ApJ, 598, 858
Massey, P., Neugent, K. F., Hillier, J. D., & Puls, J. 2013, ApJ, 768, 6
Meier, D. L., & Terlevich, R. 1981, ApJ, 247L, 109
Meynet, G., Maeder, A., Schaeller, G., et al. 1994, A&A, 103, 97
Neufeld, D. 1990, ApJ, 350, 216
Palacios, A., Gebran, M., Josselin, E., et al. 2010, A&A, 516, 13
Partridge, R. B., & Peebles, P. J. E. 1967, ApJ, 147, 868
Puls, J., Vink, J. S., & Najarro, F. 2008, A&A, 16, 209
Sandberg, A., Östlin, G., Hayes, M., et al. 2013, A&A, 552, A95
Savage, B. D., & Code, A. D. 1970, in IAU Symp. 36, Ultraviolet Stellar Spectra and Related Ground-based Observations, ed. L. Houziaux & H. E. Butler (Dordrecht: Reidel), 302
Savage, B. D., & Jenkins, E. B. 1972, ApJ, 172, 491
Savage, B. D., & Panek, R. J. 1974, ApJ, 191, 659
Scarlata, C., Colbert, J., Teplitz, H. I., et al. 2009, ApJL, 704, L98
Schaerer, D. 2003, A&A, 397, 527
Schaerer, D., & Verhamme, A. 2008, A&A, 480, 369
Shapley, A. E., Steidel, C. C., Pettini, M., & Adelberger, K. L. 2003, ApJ, 588, 65
Stern, D., Yost, S. A., Eckart, M. E., et al. 2005, ApJ, 619, 12
Valls-Gabaud, D. 1993, ApJ, 419, 7
Vink, J. S. 2007, in AIP Conf. Proc. 948, Unsolved Problems in Stellar Physics (Melville, NY: AIP), 389
Walborn, N. R., Nichols-Bohlin, J., & Panek, R. J. 1985, International Ultraviolet Explorer Atlas of O-Type Spectra from 1200 to 1900 Å (NASA RP-1155)
Walborn, N. R., Parker, J. W., & Nichols-Bohlin, J. 1995, International Ultraviolet Explorer Atlas of B-Type Spectra from 1200 to 1900 Å (NASA RP-1363)